Solar Energy Materials & Solar Cells 110 (2013) 77–86

Contents lists available at SciVerse ScienceDirect

Solar Energy Materials & Solar Cells

journal homepage: www.elsevier.com/locate/solmat

# A two-diode model regarding the distributed series resistance

O. Breitenstein *, S. Rißland

*Max Planck Institute of Microstructure Physics, Halle, Germany*

ARTICLE INFO

*Article history:*
Received 20 August 2012
Received in revised form
23 November 2012
Accepted 26 November 2012

*Keywords:*
Characterization
Two-diode model
Current–voltage characteristic
Simulation
Fit

ABSTRACT

The two-diode model is widespread for interpreting dark and illuminated current–voltage characteristics of solar cells, though it does not hold correctly for high current densities due to the distributed character of the series resistance. This is one reason for the fact that fitting the dark and the illuminated characteristic leads to two different sets of two-diode parameters. After locally analyzing a typical multicrystalline solar cell, it is found that here the grid conductivity represents the most significant contribution to the distributed series resistance. A simplified equivalent circuit implying a 1-dimensional current distribution is used for simulating current-dependent effective (lumped) series resistances in the dark and under illumination. It is found that the influence of the distributed series resistance on both characteristics can be described empirically by introducing a series resistance being variable for high currents. Moreover, well-known departures from the superposition principle often cannot be neglected. Therefore the second diode contribution is generally stronger under illumination than in the dark, and also the parallel resistance may be affected. We introduce only one additional series resistance parameter and consider that the second diode parameters and the parallel resistance may be different under illumination and in the dark. In this way, the current dependence of both the dark and the illuminated series resistance can be described with the same consistent set of first diode and series resistance parameters. Based on these findings, a two-diode model with an analytically given variable series resistance is proposed, which may describe both the dark and the illuminated characteristic up to large current densities in good approximation with one and the same physically meaningful parameter set.



## 1. Introduction

The dark and the illuminated current–voltage ($I$–$V$) characteristic of solar cells are usually described by the two-diode or double-diode model, where the first diode describes the so-called diffusion current having an ideality factor of unity, and the second diode describes the current due to recombination in the depletion region. For the latter current contribution often an ideality factor of 2 is assumed, but for many solar cells the ideality factor is found to be larger than 2. Whereas the local diffusion current density is closely related to the effective local minority carrier lifetime in the bulk and the recombination properties of the surfaces, the recombination current (just like the ohmic shunt current contribution due to the parallel shunt resistance $R_p$) does not show this correlation but flows mainly in local positions like the cell edge or other extended defects crossing the p–n junction [1]. The homogeneously flowing recombination current density according to established diode theory [2] is usually about two orders of magnitude smaller than the measured average recombination current density. Thus, in crystalline silicon solar cells, also in multicrystalline (mc) ones, the major contribution of the recombination current flows in some local "non-linear shunt" positions, like the edge region, and in the overwhelming part of the area the diffusion current dominates [1]. Therefore the ideality factor under low injection condition is indeed close to unity in most parts of the area, if the lifetime is not dependent on the minority carrier concentration [3]. The large ideality factor of the recombination current can be attributed to multi-level recombination [4].

A decisive parameter of a solar cell is its series resistance. In the conventional two-diode model one series resistance $R_s$ is used for all three current contributions (diffusion, recombination, and ohmic). For becoming independent of the cell area, it is usual to express all currents as current densities and $R_s$ as an "area-related" series resistance, given in units of $\Omega\,cm^2$. Originally, this definition was probably based on the assumption of a homogeneous current flow and a homogeneous voltage drop across the whole cell area. Only then the global (lumped) series resistance equals the area-related $R_s$ divided by the cell area. However, this definition is also applicable to an inhomogeneous current distribution and locally varying series resistance by defining the

* Correspondence to: Max Planck Institute of Microstructure Physics, Weinberg 2, 06120 Halle, Germany. Tel.: +49 345 5582740; fax: +49 345 5511223.
*E-mail address:* breiten@mpi-halle.mpg.de (O. Breitenstein).

0927-0248/$ - see front matter © 2012 Elsevier B.V. All rights reserved.
http://dx.doi.org/10.1016/j.solmat.2012.11.021

local series resistance as the local voltage drop divided by the local current density, as it is being done by most authors. The most successful method for imaging this local series resistance quantitatively is based on photoluminescence (PL) imaging [1,5]. The concept of an area-related series resistance assumes that each region (mapped by a single camera pixel) of a cell is connected to the cell terminal by its own individual series resistance. Thus, this concept actually assumes that the metallization and the emitter have a negligible resistance (all positions show the potential of the terminal), and that the series resistance appears at the vertical current flow through the cell. It is well known that this is by far not the case. Instead, all currents flowing horizontally in the cell may lead to a distributed series resistance [6,7]. Hence, in each position the voltage drop due to the horizontal current is not only due to the vertical diode current flowing in this position, but also due to diode current contributions from the whole lateral current path to the terminal. Moreover, the different types of current contributions (diffusion, recombination, and ohmic) are distributed inhomogeneously and do not correlate with each other [1], which will be discussed in Section 4. The goal of this contribution is an easy way to implement the distributed series resistance into the two-diode model. This model will work only for a typical 'regular' solar cell not showing e.g. extended regions of high series resistance.

If the diode current flows only in the position of the considered pixel and the current density in the rest of the cell is zero (no illumination), the horizontal path resistance between this pixel and the two grid lines or busbars will depend on the lateral position. It is zero at the two terminals (grid lines or busbars, respectively) and shows a maximum in the middle. As it will be shown in the next section, the dependence of this resistance on position is also a parabola, like for the distributed $R_s$ under illumination. We propose to name this type of local dark resistance "geometrical shunt resistance", since it holds for a local current flow only in this position (which is conventionally called a 'shunt') if the homogeneous current density in its surrounding is negligibly small. We will analyze this geometrical shunt resistance in the context of an area-related resistance in the next section. Our definition of the local resistance contribution, which is induced by the distributed series resistance, already includes this geometrical effect.

There have been numerous publications dealing with the distributed series resistance effect, see e.g. [6–10]. They are often based on a 2-D solar cell model which has to be evaluated numerically. Hence, it is not easy to extract the device parameters from measured *I–V* characteristics. Fischer et al. [7] have proposed to combine all distributed $R_s$ components into one parameter and to fit the dark and illuminated characteristics to a 1-dimensional cell model. However, this approach is not directly related to the two-diode model, and for its evaluation a special software is necessary. The approach proposed in this work is related to that used in [7], but we finally describe the high-current phenomena by an analytically given current-dependent series resistance. In a recent work, Fong et al. have measured current- and voltage-dependent series resistances for a set of monocrystalline silicon cells, based on the multi-light method [11]. Their approach is not based on the two-diode model and they do not use an analytical description of their results. In the present paper, based on the analytic results presented in [6] and model B of [7], we use analytic approaches to describe the current-dependent series resistance in the dark and under illumination and use them in the conventional two-diode model instead of the usual constant series resistance $R_s$. Following [10] we determine the basic two-diode parameters from evaluating the dark characteristic at low currents and then vary the fixed and the distributed part of $R_s$ until the whole dark characteristic is well described. For describing the illuminated characteristic, the bulk recombination-induced departure from the superposition principle after Robinson et al. [12] is considered by an additional contribution to the second-diode current. It is described there that even the measured ohmic parallel conductance may be influenced by this effect. This approach provides a practicable method to describe dark and illuminated *I–V* characteristics up to high current densities by a consistent simple and physically meaningful parameter set.

In Section 2, we first describe the main issues for a correct *I–V* curve measurement, which is necessary for an evaluation of the two-diode parameters. Then in Section 3 a typical industrial solar cell is locally analyzed with respect to its distributed series resistance, based on an $R_s$ image obtained from electroluminescence (EL) measurements, and the simulation of the distributed $R_s$ used in this work is explained. In Section 4 the one-dimensional simulation is performed for various cell parameters, and the simulated results are described by an analytic model of a variable lumped $R_s$. Finally, in Section 5 the experimental dark and illuminated characteristics of a typical cell are fitted to this model.

## 2. Experimental

The measurement of the *I–V* characteristics was done on a self-constructed water-cooled measurement chuck made from copper. The cell is sucked on the chuck by a vacuum and is biased by a four quadrant power supply. It enables a homogeneous contact of the rear side of the solar cell, while each front side busbar is contacted by six spring-loaded pins mounted along a low-ohmic rail. It is essential for the investigation that no additional series resistance due to the contact scheme is measured. Therefore a four-probe contact scheme is used, which includes additional sense pins contacting the middle of each front side busbar and one pin sensing the rear side contact. An identical contact scheme was also used for measuring the EL-images.

Especially for the measurement of the illuminated *I–V* characteristic it has to be ensured that the temperature of the solar cell does not increase due to the irradiated power. Therefore an independent measurement of the solar cell surface temperature was obtained by an IR-thermometer. Under illumination, the temperature of the chuck was decreased until the temperature of the cell reaches 25 °C.

## 3. Local resistance analysis

As mentioned above, the traditional approach to image the local series resistance in solar cells defines the local $R_s$ as the voltage drop between the cell terminals and the local diode bias, divided by the local current density [5,13–16]. Though this definition of $R_s$ does not consider its distributed character, the resulting $R_s$ images correctly describe the local voltage distribution at the p–n junction at the biasing condition of the $R_s$ imaging, if the local current density is known. However, for other biasing conditions, slightly different $R_s$ images may be necessary to describe the local voltage distribution. A quite simple method for measuring the local series resistance is EL $R_s$ [14,16], where two EL images measured at two different biases are evaluated. The necessary scaling factor $f$ included in this analysis may be chosen such that the averaged $J_{01}$ equals the global value taken from the dark *I–V* characteristic. It will be discussed below that there are clear indications that the ideality factor of the diffusion current may be somewhat larger than unity for multicrystalline solar cells. Therefore we have extended the theory for quantitatively evaluating EL images [16] by considering an ideality factor

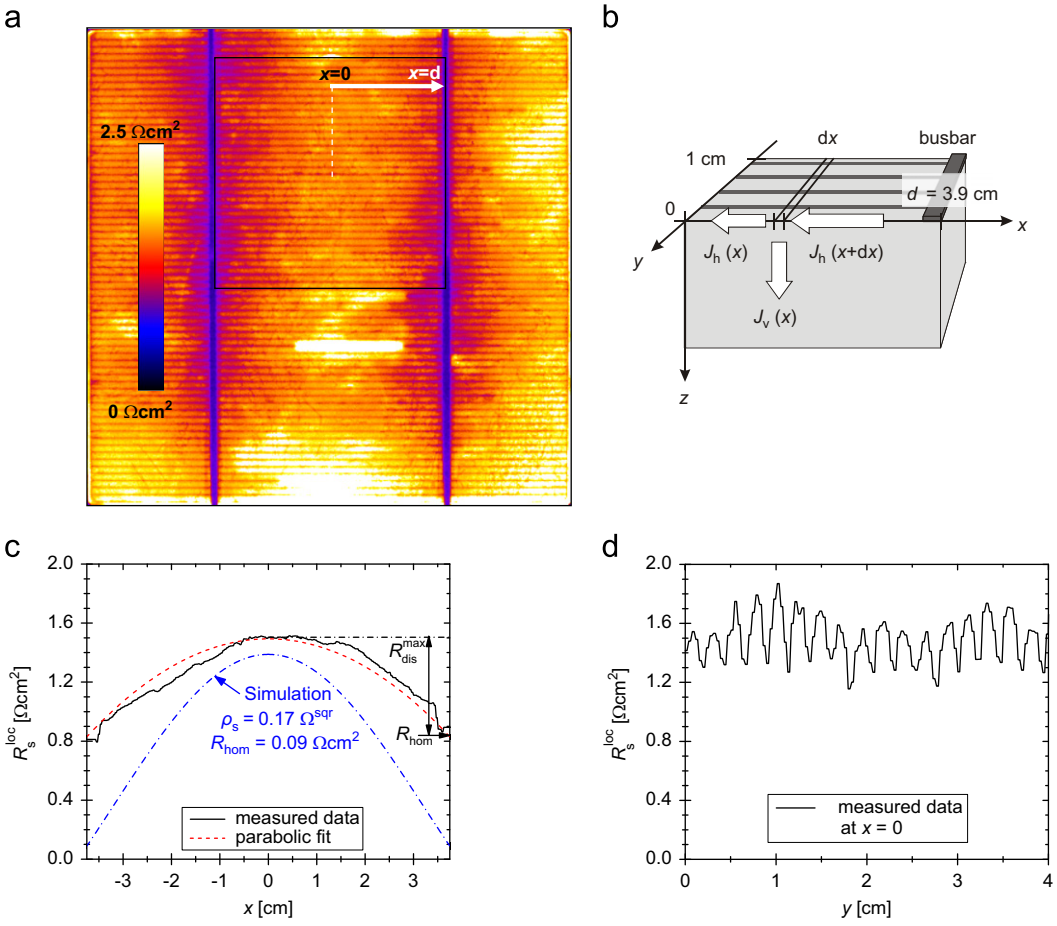


**Fig. 1.** (a) EL $R_s$ image of the whole investigated cell ($n_1=1.06$), (b) investigated symmetry element with $J_v$ being the vertical and $J_h$ the horizontal current density (without illumination), (c) averaged EL $R_s$ profile of the marked region between the two busbars in horizontal direction, together with the parabolic data fit (red dashed line) and the profile expected from the evaluation of the $I$–$V$ curve (blue dash-dotted), (d) $R_s$ profile in $y$ direction at $x=0$ (dotted line in (a)). (For interpretation of the references to color in this figure legend, the reader is referred to the web version of this article.)

of the diode current different from unity [17]. Fig. 1(a) shows the EL $R_s$ image of a typical industrial multicrystalline solar cell based on the evaluation of EL images taken at 548 and 597 mV by assuming an ideality factor of 1.06, which will be justified below. Qualitatively, this series resistance looks very similar to that by assuming an ideality factor of 1, only the quantitative values depend on the chosen ideality factor. The cell investigated here was made from a multicrystalline 15.6 cm × 15.6 cm sized wafer produced by the Bridgeman technique and holding a resistivity of 1–2 Ωcm. It was manufactured by an industrial process including acidic texture, a front grid design with two busbars, and full-area Al-alloyed back contact. The solar cell shows $V_{oc}=612$ mV, $J_{sc}=33.1$ mA/cm$^2$, $FF=76.8$ %, and an energy conversion efficiency of $\eta=15.6$ %. Since there are just a few irregularities of $R_s$ between the busbars, the marked region in Fig. 1(a) may be considered as typical for this type of cells. In Fig. 1(b) the symmetry element used in the later simulation is sketched and the electron currents are indicated. Fig. 1(c) shows the averaged horizontal $R_s$ profile of the region selected in (a) (from busbar to busbar), and (d) shows the vertical $R_s$ profile across the grid lines taken in the middle of the cell as marked in (a) by the dotted line. A comparison of (c) and (d) shows that the strongest spatial variation of $R_s$ of 0.66 Ω cm$^2$ is in horizontal (grid) direction, where the lateral series resistance is dominated by the resistance of the grid lines. The variation of $R_s$ in vertical direction (from grid line to grid line) due to the emitter sheet resistance is smaller (see Fig. 1(d)). It even can be expected that the local $R_s$ minima in grid positions are, at least partly, caused by a shadowing effect. Thus, the distributed series resistance caused by the emitter resistivity is obviously not the dominant contribution to the distributed $R_s$, which is in contrast to the assumptions made e.g. in [6,7,11]. Qualitatively similar series resistance images of 'regular' solar cells, showing a stronger $R_s$ variation from busbar to busbar than from grid line to grid line, have been obtained also by other authors [1,13,14,16]. It can therefore be expected that the description of the distributed $R_s$ of the whole cell by a one-dimensional model regarding only the grid line resistance may describe the dominant contribution to the distributed $R_s$.

First, for the one-dimensional case sketched in Fig. 1(b) the local geometrical shunt resistance according to the definition given above will be calculated. Hence, here we assume that only in a position $x$ between two terminals with a distance $2d$ a vertical current flows. This is equivalent to a shunt line in $y$ direction parallel to the busbars in the dark, carrying this current, which may be e.g. a scratch parallel to the bus bars. The advantage of this shunt geometry, in comparison to a point shunt, is that it is easy to analyze and avoids any singularity. The series resistance to this line (referred to a shunt stripe of width of $w=1$ cm) is the parallel circuit of the series resistances to the left and the right busbar:

$$\frac{1}{R_s^{geo}} = \frac{w}{\rho_s(d+x)} + \frac{w}{\rho_s(d-x)}$$

$$R_s^{geo} = \rho_s \frac{d^2-x^2}{2wd} \qquad (1)$$

$\rho_s$ is the sheet resistance of the device, here governed by the grid lines. This dependence is parabolic, it is zero at $x=+/-d$, and

its maximum value at $x=0$ is given by $\rho_s d/2w$. If this resistance has to be expressed as an area-related resistance (in units of $\Omega\,cm^2$), it has to be multiplied by $w \times dx$, with $dx$ being the width of the shunt line. The maximum value at $x=0$ becomes

$$R_{geo}^{max} = \rho_s \frac{d dx}{2} \tag{2}$$

Interestingly, the area-related resistance to a local shunt depends on its geometry, the smaller the shunt area, the lower is the area-related resistance to it. This was observed already in [1], where the dark resistance image measured by the RESI method [15] showed local minima in shunt positions, in contrast to the illuminated resistance image measured by PL [5], which is measured under homogeneous current flow condition. On the other hand, if the vertical current density outside of this shunt is zero, but the voltage drop is obviously not, in this region the area-related series resistance is infinite. In reality the current is not zero outside of the shunts, neither in the dark nor under illumination, therefore also there the area-related series resistance remains finite. Nevertheless, the general tendency remains: If there is a local shunt where the current density is significantly higher than in its surrounding, in shunt position the area-related series resistance (in conventional definition) decreases, whereas in its surrounding it increases, because of the action of the distributed series resistance. For point shunts we have, in addition, the current crowding effect, which again increases the series resistance with decreasing shunt area. This whole situation is not intuitively expected, since it contradicts the idea of a current-independent series resistance network. The nominal series resistance decrease in shunt position is here only due to the conventional area-related definition of $R_s$, which does not hold for any horizontal current flow. As (1) shows, the real resistance to this line shunt is constant and independent of $dx$. This situation may be called the shunt paradox.

For homogeneous sheet resistance and diode parameters, if the voltage drop at a distributed series resistance is small compared to the thermal voltage $V_T = kT/e$ (low current in the dark or low illumination intensity) and the vertical current density is homogeneous, a pure 1-dimensionally distributed series resistance can still be treated analytically, as it has been shown e.g. in [6,7]. In contrast to the procedure described there, we select $x=0$ in the middle between the busbars and $x=d$ in busbar position, with the active element length $d$ being half of the distance between two busbars (see $x$ axis in Fig. 1(a) and (b)), which simplifies the mathematical treatment. If the horizontal resistance in the emitter layer is dominated by the grid resistance, its equivalent sheet resistance in $x$ direction is $\rho_s = R_{grid} \times D$, with $R_{grid}$ being the grid resistance (in units of $\Omega$/cm) and $D$ the distance between two grid lines, here being $D=0.233$ cm. If $J_h(x)$ is the horizontal current density at position $x$ (in units of A/cm) and $J_v(x)$ is the vertical diode current density in this position (in units of A/cm$^2$), in every position $x$ holds:

$$\frac{\partial V(x)}{\partial x} = V'(x) = -\rho_s J_h(x) \tag{3}$$

$$\frac{\partial J_h(x)}{\partial x} = -J_v(x) \tag{4}$$

leading to

$$\frac{\partial^2 V(x)}{\partial x^2} = V''(x) = \rho_s J_v(x) \tag{5}$$

With the starting condition $V(0)=V_0$, $V'(0)=0$, and $J_v(x)=$constant (low current density), Eq. (5) may be easily integrated over $x$, leading to the well-known parabolic voltage profile:

$$V(x) = V_0 + \frac{1}{2}\rho_s J_v x^2 \tag{6}$$

$V(d) = V_0 + \rho_s J_v d^2/2$ is the terminal (bias) voltage $V_B$. Based on the conventional definition of an area-related series resistance, the local resistance due to this distributed series resistance is:

$$R_{dis}(x) = \frac{V(d)-V(x)}{J_v} = \frac{\rho_s}{2}\left(d^2 - x^2\right) \tag{7}$$

The maximum local resistance at $x=0$ due to the distributed resistance is

$$R_{dis}^{max}(x) = \frac{\rho_s d^2}{2} \tag{8}$$

This has to be compared with the maximum of the (area-related) geometrical shunt resistance (1), which would hold if the vertical current flowed only in the considered local position and there was no vertical current flow outside of this region. Since $dx \ll d$ holds, this geometrical resistance is always small compared to the distributed resistance described above and does not have to be confused with that.

The average (effective, lumped) distributed series resistance is obtained by averaging (7) from 0 to $d$, leading to:

$$R_{dis} = \frac{1}{3}\rho_s d^2 \tag{9}$$

The area-related resistance $\rho_s d^2$ has been called "geometrical resistance" in [6] and "$R_{CC}$" in [7]. We will refer to (9), including the factor 1/3, as the (area-related) "global distributed series resistance" $R_{dis}$ of this cell. For low voltages resp. currents, this resistance simply adds to a spatially homogeneous (not distributed) series resistance $R_{hom}$.

If high cell current values are considered, the voltage drop at the distributed series resistance is not small compared to $V_T$ anymore, $J_v(x)$ becomes dependent on $x$, and (6) cannot be easily integrated analytically. However, based on (3) to (5), a simple yet accurate numerical analysis is possible using the geometry of Fig. 1(b). We are using model (B) of [7], hence in each position $x$ we assume, in addition to the distributed resistance, a homogeneous resistance $R_{hom}$ in series with the local diode, which is only described by its saturation current density $J_{01}$ and its ideality factor $n_1$, here taken as $n_1=1$. As mentioned above, the current contributions of $J_{02}$ and $R_p$ are not flowing homogeneously and need not be considered here. Then the local vertical current density is described by the following implicit equation ($J_{sc}$ being the short circuit current density under illumination, the dark case is $J_{sc}=0$):

$$J_v(x) = J_{01}\,\exp\frac{V(x) - R_{hom} \times J_v(x)}{n_1 \times V_T} - J_{sc} \tag{10}$$

We restrict our treatment of the distributed resistance to its contribution due to the grid finger resistance, which is described by an effective sheet resistance $\rho_s$ and a path length $d$ leading to an effective global distributed resistance of $R_{dis} = \rho_s d^2/3$. This is, of course, only a first approximation, since eventual contributions of the emitter resistivity to the distributed resistance are not explicitly considered yet. Following Fischer et al. [7] we expect that this contribution may finally be regarded by increasing the amount of the effective global distributed series resistance of the whole cell, which will be discussed below. For the numerical evaluation of (3) to (5) we split the integration path from $x=0$ to $d$ into equidistant fractions of length $dx$ and assume that the vertical current density $J_v(x)$ is constant within each fraction. Then the voltage profile between two positions $x$ and $x+dx$ is a quadratic function, for which the following relations hold:

$$V(x+dx) = V(x) + V'(x)dx + \frac{V''}{2}dx^2 \tag{11}$$

$$V'(x+dx) = V'(x) + V''(x)dx \tag{12}$$

The starting boundary conditions at $x=0$ are

$$V(0)=V_0 \quad V'(0)=0 \quad J_h(x)=0 \tag{13}$$

Starting from $x=0$, step by step the local voltage $V(x)$ and its gradient $V'(x)$ are calculated for the next position $x+dx$ by using $V'$ of (3) and $V''$ of (5). In each position $J_h(x)$ is incremented using (10) according to

$$J_h(x+dx)=J_h(x)+J_v(x)dx \tag{14}$$

Note that here the integration direction is opposite to the electron current direction (arrows in Fig. 1(b)) and we consider dark conditions, therefore both $V'$ and $V''$ are positive. The calculation of $J_v(x)$ according to (10) is the only step that cannot be performed analytically. We have made all calculations by using Mathematica [18]. It was found that, for d$x$ smaller than 0.05 mm, the result did not depend on d$x$ anymore. Since for our cell the distance of the edges to the busbars was slightly larger than half the distance between the busbars, we simulate the given solar cell structure with $d=3.9$ cm, being slightly different to $d=3.75$ cm measured at the cell. $V(d)$ is the cell bias $V_B$ and $J_h$(d) is the current of a 1 cm wide and $d=3.9$ cm long stripe. For obtaining the current $I(V)$ of the whole cell with an area of $A=15.6\times15.6=243.4$ cm$^2$, the current of one symmetry element has to be multiplied by a factor of $A/(3.9\ \text{cm}^2)$. Repeating this whole procedure for various starting voltages $V(0)$ yields the complete $I$–$V$ characteristic. Fig. 2(a) shows the vertical current profiles and (b) the voltage profiles in the dark calculated in this way for a cell having typical series resistance parameters of $R_{hom}=0.2\ \Omega\ \text{cm}^2$ and $R_{dis}=0.7\ \Omega\ \text{cm}^2$. We assume $J_{01}=1.48\times10^{-12}$ A/cm$^2$ and $J_{sc}=33.1$ mA/cm$^2$, as for our cell assuming $n_1=1$ and plot the data for two biases of $V=0.5$ and 0.639 V, where a dark current corresponding to $I_{sc}$ flows. We see that at 0.5 V bias the current density is still homogeneous, but at 0.639 V the current density varies spatially by a factor of almost 3 and the local voltage by 31 mV due to the distributed series resistance. Calculating the local series resistance profile between the busbars by dividing the voltage drop at each position through the local current density $J_v(x)$ leads to a parabolic characteristic for almost homogeneous currents at 500 mV as predicted by Eq. (7). In the high current case at 639 mV, the curve follows a clearly different behavior with a higher series resistance in the inner part of the cell and a lower $R_s$ near the busbars (see Fig. 2(c)). This is a consequence from the changed current paths, namely that (in the dark) at high voltage the injection occurs preferredly close to the busbars resp. grid lines.

## 4. The current-dependent lumped series resistance

The numerical simulation of the $I$–$V$ characteristics described above has been performed in the dark and under 1 sun illumination for various values of the effective global distributed and homogeneous series resistance. Then the obtained characteristics have been interpreted using a set of ideal one-diode models with differing $R_s$ values in order to determine the current-dependent lumped $R_s$ for the whole device. For that, for each current density value it has been checked which lumped $R_s$ in an ideal one-diode model (assuming homogeneous current flow in the whole area) leads for this current to the same terminal voltage. The results of these simulations are shown for some typical parameters by the symbols in Fig. 3. As it has been shown previously [6,7], the dark lumped $R_s$ reduces with increasing current density, and the illuminated $R_s$ increases. These results completely agree with that of Fig. 4 in [6], where the data under illumination are displayed as a function of $J_{sc}$ and not of the terminal current. These simulations were performed assuming an ideality factor of $n_1=1$. In the final results a deviating ideality factor is regarded by multiplying the thermal voltage $V_T$ by $n_1$.

Araújo et al. [6] have derived analytical expressions for the current-dependent $R_s$ due to a distributed series resistance. However, for the illuminated case, they only derived expressions for $R_s$ as a function of the short circuit current density $J_{sc}$ under special illumination conditions (open and short circuit). Interestingly, these expressions do not depend on diode parameter $J_{01}$ but only on the current density $J$, since the value of $J_{01}$ only affects the amount of the diode voltage, but not the voltage drop at $R_s$. For the illuminated series resistance under open circuit condition (as a function of $J_{sc}$) they derived an expression given in Eq. (20) of their paper [6]. We have found that, by introducing a scaling factor of 1.6 for the current density, this formula nicely approximates our and their numerically obtained current-dependence of the dark $R_s$, including the limiting values for high and low current densities for arbitrary values of $R_{hom}$ and $R_{dis}$. Including the ideality factor $n_1$, the final expression reads

$$R_s^{dark}=\frac{\theta_{dark}}{\tanh(\theta_{dark})}R_{hom}+\left(\frac{\theta_{dark}}{\tanh(\theta_{dark})}-1\right)\frac{n_1V_T}{1.6J} \tag{15}$$

$$\theta_{dark}=\sqrt{\frac{3R_{dis}}{R_{hom}+(n_1V_T/1.6J)}}$$

This dependence is shown in Fig. 3 as solid lines labeled "empirical dark". For all parameters these lines nicely fit the

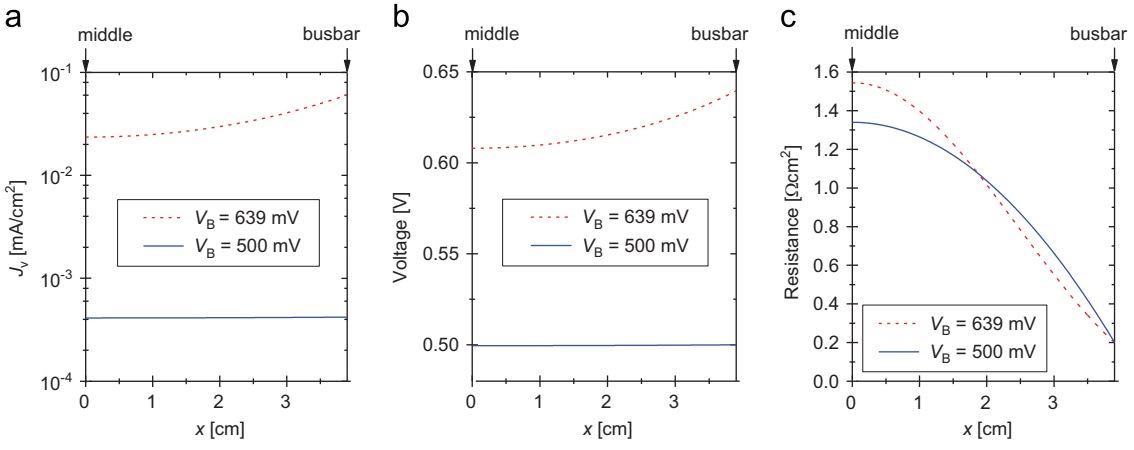


**Fig. 2.** Vertical current, voltage, and series resistance profile from the middle of the cell to a busbar for two bias voltages without illumination.

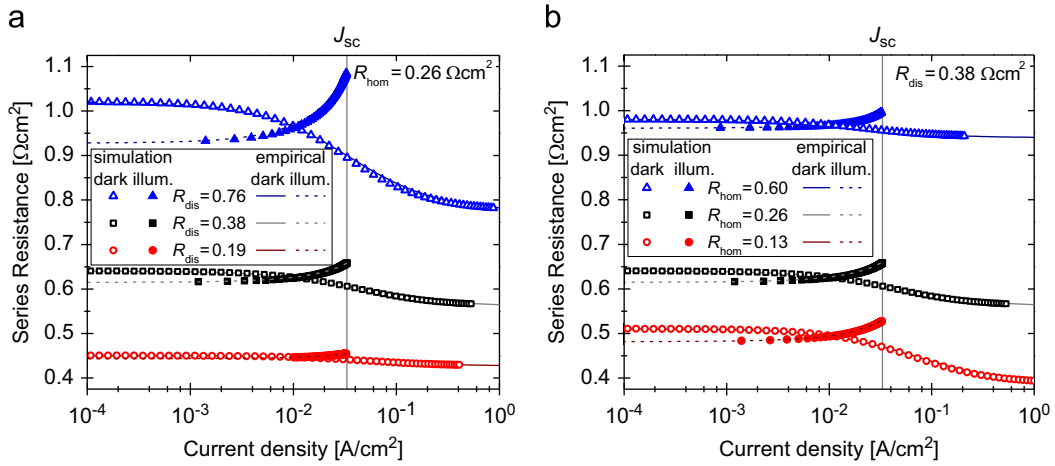


**Fig. 3.** Numerically simulated and empirically fitted dependence of the series resistance of the current density for different values of $R_{dis}$ (a) and $R_{hom}$ (b), $J_{sc}$ = 33.1 mA/cm² assumed.

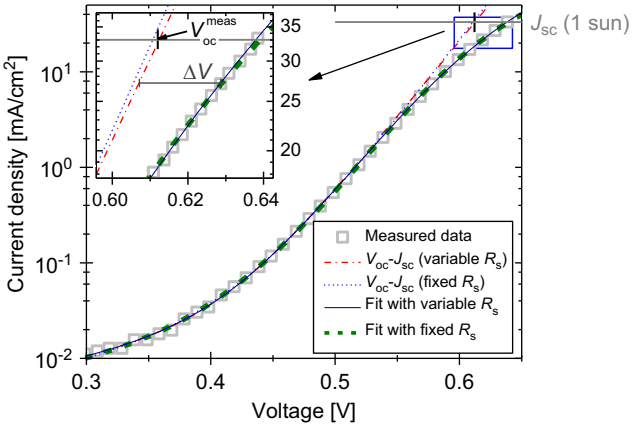


**Fig. 4.** Measured and simulated dark *I–V* characteristics with current-dependent $R_s$ (solid, blue) and fixed $R_s$ (dashed, green) as well as the corresponding simulated $J_{sc}$–$V_{oc}$ curves and the measured $V_{oc}$. (For interpretation of the references to color in this figure legend, the reader is referred to the web version of this article.)

numerically obtained values. For the illuminated case, Araújo et al. [6] have derived expressions for the open circuit and the short circuit case (Eqs. (20) and (21) in [6]). By interpolating between these two cases, we propose the following expression for the current-dependent $R_s$ under illumination, again including the ideality factor $n_1$:

$$R_s^{ill} = \frac{\theta_{ill}}{\tanh(\theta_{ill})} R_{hom} + \left(\frac{\theta_{ill}}{\tanh(\theta_{ill})} - 1\right) \frac{n_1 V_T}{J_{sc} - J} + \left(\frac{J}{J_{sc}}\right)^{\beta} \left[\frac{-n_1 V_T}{J_{sc}} \ln\left(\frac{2\alpha}{\sqrt{\pi}\,\mathrm{erf}(\alpha)}\right) + \frac{1}{2} R_{dis}\right] \quad (16)$$

$$\theta_{ill} = \sqrt{\frac{3R_{dis}}{R_{hom} + (n_1 V_T)/(J_{sc} - J)}} \quad \alpha = \sqrt{\frac{3R_{dis} J_{sc}}{2 n_1 V_T}} \quad \beta = 1 + \frac{R_{hom} J_{sc}}{1.5 n_1 V_T}$$

Also this dependence matches the limiting values for high and low current densities for arbitrary values of $R_{hom}$ and $R_{dis}$ reported by Araújo et al. [6]. This dependence is also shown in Fig. 3 as dashed lines labeled "empirical illum.". These lines nicely fit the numerically obtained values for all chosen parameters, too.

## 5. Application to measured *I–V* characteristics

The previous simulations only regarded the ideal diode current (diffusion current, assumed to be homogeneous) but did not take into account any depletion region recombination current nor an ohmic shunt current. It has been discussed already in Section 1 that these different current contributions are flowing in different positions, only the diffusion current is flowing more or less homogeneously, depending on the local bulk lifetime, but the other two current contributions are flowing in certain (usually different) local positions. Thus, actually the different components should be described by different $R_s$ values, as it had been proposed e.g. in [19]. On the other hand, the depletion region recombination and the ohmic component usually dominate at low voltages where the influence of the series resistance is low. Therefore, for not unnecessarily increasing the number of parameters, here we will apply one and the same current-dependent series resistance to the total cell current.

**Table 1**
Comparison of $R_s$ data obtained from evaluating EL data and different evaluations of the dark and illuminated characteristics.

| Parameter | EL $R_s$ | Constant $R_s$ from *I–V* curve | Current-dependent $R_s$ |
|---|---|---|---|
| $R_{dis}$ [Ω cm²] | 0.48 ± 0.02 | | 0.87 ± 0.17 |
| $R_{hom}$ [Ω cm²] | 0.83 ± 0.02 | | 0.09 ± 0.08 |
| $R_s^{dark}$ ($J_{sc}$) [Ω cm²] | 1.28 ± 0.04 | 0.85 | 0.77 ± 0.01 |
| $R_s^{ill}$ ($J_{sc}$) [Ω cm²] | 1.34 ± 0.04 | 1.17 | 1.04 ± 0.11 |

First we will try to fit the EL-based series resistance data from Fig. 1 to the linear one-dimensional model, having in mind that this can only be a coarse approximation since (6)–(8) only hold in the low-current limit, which certainly does not hold for the current above 2.6 A used for the EL measurements. As indicated in Fig. 1(c), the measured EL $R_s$ resistance profile can be modeled reasonably by assuming $R_{hom}$ = 0.83 Ω cm² plus a distributed sheet resistance leading to $R_{dis}^{max}$ = 0.66 Ω cm². According to (8) and (9) this would correspond to a global $R_{dis}$ = 0.442 Ω cm², hence at low currents the series resistance is expected to be about $R_{hom} + R_{dis}$ = 1.272 Ω cm². Regarding the active length of $d$ = 3.75 cm of the symmetry element in Fig. 1(b), this $R_{dis}$ corresponds to a sheet resistance of $\rho_s$ = 0.094 $\Omega^{sqr}$. Applying this value to our model with the slightly different $d$ = 3.9 cm (since the distance of the edges to the busbars was larger than half the distance between the busbars) will increase the $R_{dis}$ to 0.478 Ω cm² as indicated in Table 1. For a grid distance of $D$ = 0.233 cm $\rho_s$ leads to a grid resistance of $R_{grid} = \rho_s/D$ = 0.405 Ω/cm. We also have measured the total resistance between the two busbars to be 0.0415 Ω. 67 grid lines in parallel with 7.3 cm length leads

to $R_{grid}=0.380\,\Omega$/cm. This agrees reasonably to $R_{grid}=0.405\,\Omega$/cm estimated by evaluating the series resistance profile in Fig. 1(c). General uncertainties of the EL-based $R_s$ imaging results will be discussed below.

The next task is to fit the dark characteristic to our variable resistance model, and then these results will be used to fit also the illuminated characteristic. At the beginning the low-current part of the characteristic (up to 3 mA/cm$^2$) is fitted to the two-diode model in the conventional way. This curve fitting was performed by using a code kindly provided by Greulich (Fraunhofer ISE, Freiburg, Germany), which was also used in [10]. In this current range the series resistance is still almost constant (see Fig. 3) and the general influence of $R_s$ is still weak. A value of $R_s$ eventually appearing from this fit represents the sum of $R_{hom}$ and $R_{dis}$, but this number shows a large uncertainty since the voltage drop at $R_s$ is very low. By this fit the parameters $J_{01}$, $J_{02}$, $n_2$, and $R_p$ are obtained with sufficient accuracy. Knowing these parameters, the open circuit voltage $V_{oc}$ may be obtained, which is independent of $R_s$. If we do this with the data of our cell assuming $n_1=1$, $V_{oc}$ appears about 5 mV smaller than measured. This deviation may be caused by an injection level-dependent lifetime in the bulk, which leads to an ideality factor of the diffusion current of $n_1>1$ [3,20]. Indeed, by assuming $n_1=1.06$ in the two-diode parameter fit, the correct value of $V_{oc}$ can be simulated from the dark characteristic. This procedure for obtaining $n_1$ is much more accurate than using $n_1$ as an independent fitting parameter in the two-diode fit. Note, however, that the assumption of $n_1>1$ changes the magnitude of $J_{01}$ significantly, which is then not comparable with $J_{01}$-values obtained conventionally by assuming $n_1=1$ anymore. This ideality factor of $n_1=1.06$ was also used for calculating the $R_s$ image from two EL images taken at 0.548 and 0.597 V [17]. Note also that care must be taken at the $I$–$V$ characteristic measurements for ensuring that all characteristics are measured at a cell temperature of 25 °C, e.g. by performing the illuminated measurements at a chuck temperature slightly lower than 25 °C to compensate the heating of the cell during the measurement. The difference between an ideality factor of 1.0 and 1.06 corresponds to a temperature difference of about 18 K.

Now, knowing the two-diode parameters, for all current densities $J>3$ mA/cm$^2$ the diode voltages $V_{diode}(J)$ (without the influence of $R_s$) may be calculated. The resulting $J_{sc}$–$V_{oc}$ (suns-$V_{oc}$) curve is plotted as red dash-dotted line in Fig. 4. Together with the measured dark characteristic $J_{dark}(V)$, resp. $V_{dark}(J)$, the current-dependent lumped $R_s$-values are evaluated according to:

$$R_s(J)=\frac{V_{dark}(J)-V_{diode}(J)}{J} \tag{17}$$

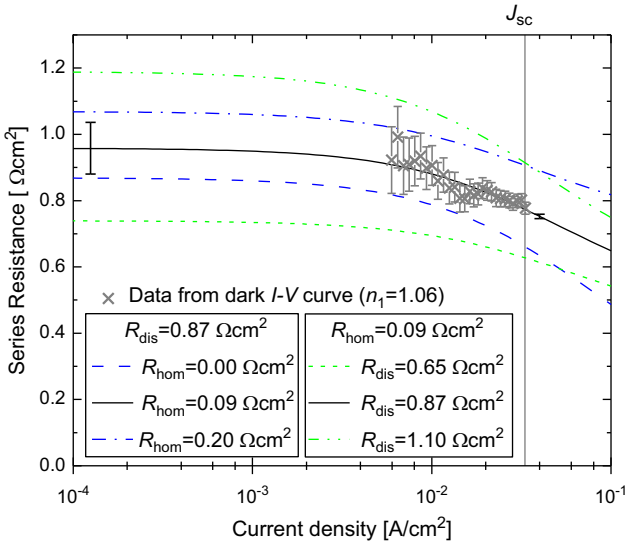


**Fig. 5.** Evaluated current-dependent dark series resistance from the measured dark $I$–$V$ curve under the assumption of a diffusion current ideality factor $n_1=1.06$ leading to the correct $V_{oc}$.

Fig. 5 shows the result of this procedure for our cell, together with the dependencies expected by (15) for several sets of the parameters $R_{hom}$ and $R_{dis}$. It turns out that the resistance parameters obtained in Section 2 by evaluating the EL-based $R_s$ image do not lead to the optimum fit. Instead, $R_{dis}$ is more and $R_{hom}$ is less pronounced in the $I$–$V$ characteristics evaluation, compared to the EL evaluation. This leads to values of $R_s^{dark}(J_{sc})$ and $R_s^{ill}(J_{sc})$ which are just about 60 % to 77 % of the values estimated from the EL evaluation. These deviations will be discussed later. The optimum fit parameters for the dark characteristic are given in Table 1 and Table 2. The resulting fit of the measured dark $I$–$V$ characteristic is plotted as a solid blue line in Fig. 4. Additionally, the measured dark $I$–$V$ data (including the high current values) were fitted conventionally assuming a constant $R_s$ and $n_1=1$. The obtained parameters are also given in Table 2. The fit with this fixed $R_s$, shown in Fig. 4 as a green dashed line, does not significantly deviate from our fit using a variable $R_s$. However, as the data in Table 2 show, for a fixed $R_s$ the data of $R_s$ and of $J_{01}$ significantly differ between dark and illuminated characteristics. As it becomes visible in the inset of Fig. 4, the $J_{sc}$–$V_{oc}$-curve corresponding to the fit with the fixed $R_s$ and $n_1=1$ (blue dotted line) results in a slightly lower $V_{oc}$ than measured, which is also indicated by an arrow in this inset.

**Table 2**
Two-diode parameters obtained for dark and illuminated $I$–$V$ characteristics with current-dependent $R_s$ and fixed $R_s$ as well as the corresponding illuminated $I$–$V$ characteristics simulated by these parameters.

| Parameter | Measured (850 nm) | Fixed $R_s$ | | Variable $R_s$ | | |
|---|---|---|---|---|---|---|
| | | Dark | Illuminated | Dark | 0.1 sun | 1.0 sun |
| $J_{01}$ [A/cm$^2$] | | $1.50\times10^{-12}$ | $1.36\times10^{-12}$ | $5.57\times10^{-12}$ | $5.57\times10^{-12}$ | $5.57\times10^{-12}$ |
| $n_1$ | | 1.00 | 1.00 | 1.06 | 1.06 | 1.06 |
| $J_{02}$ [A/cm$^2$] | | $8.18\times10^{-9}$ | $1.17\times10^{-6}$ | $5.17\times10^{-8}$ | $1.53\times10^{-7}$ | $3.7\times10^{-6}$ |
| $n_2$ | | 2.00 | 3.65 | 2.76 | 3.2 | 4.8 |
| $R_p$ [Ω cm$^2$] | | 41855 | 18325 | 44421 | 44421 | 44421 |
| $R_s$ [Ω cm$^2$] | | 0.85 | 1.17 | | current-dependent | |
| | | Simulated illuminated $I$–$V$-curve parameters | | | | |
| $V_{oc}$ [mV] | 611.9 | 610.7 | 613.6 | 612.4 | | 612.4 |
| $J_{sc}$ [mA/cm$^2$] | 33.1 | 33.1 | 33.1 | 33.1 | | 33.1 |
| $FF$ [%] | 76.8 | 78.3 | 76.6 | 77.15 | | 76.7 |
| $\eta$ [%] | 15.56 | 15.84 | 15.56 | 15.64 | | 15.56 |

Now the illuminated characteristic will be fitted. Since we have no access to an AM 1.5 cell tester, we are using illuminated characteristics measured for various illumination intensities by homogeneous irradiation with monochromatic (850 nm) light, with the intensity chosen to match the value of $J_{sc}$ given by the producer of the cell (here 33.1 mA/cm$^2$). For evaluating these illuminated characteristics it is useful to display them logarithmically in the style of a dark characteristic by subtracting $J_{sc}$ from all illuminated current values, as it has been done also e.g. by Araújo et al. [6]. We have measured the $I$–$V$ characteristics for illumination intensities of 1 sun and of 0.1 sun and have corrected their voltages by applying the current-dependent $R_s$ values given by (16) using the already evaluated $R_{hom}$ and $R_{dis}$ given in Table 1. Note that in the presence of a finite shunt resistance $R_p$ the $J(0\,V)$ equals not $J_{sc}$ due to the voltage drop caused by $R_s$. Since in our case the illuminated $I$–$V$ characteristic is firstly corrected by $R_s^{ill}(J)$, the determined corrected $J(0\,V)$ equals $J_{sc}$ and can be used to shift the illuminated $I$–$V$ curve. The appearing error in the estimation of $J_{sc}$ due to a finite $R_p$ for the calculation of $R_s^{ill}$ in Eq. (16) is much lower than the error due to fitting $R_{hom}$ and $R_{dis}$ from the dark $I$–$V$ characteristic. Fig. 6(a) shows these $R_s$ corrected and $J_{sc}$ shifted $I$–$V$ characteristics together with the "suns-$V_{oc}$" dark characteristic, based on the measured dark characteristic with the voltages corrected by the dark $R_s$ values of (15). In comparison with the dark characteristic the illuminated $I$–$V$ curve at 0.1 sun intensity indicates a good correspondence, while there are significant deviations observable for the $I$–$V$ curve at 1 sun intensity. These deviations are so large that they cannot be explained by any errors of $R_s$ anymore, hence they are not a result of the distributed character of $R_s$. This deviation is a result of a well-known departure from the superposition principle, which had been described already in 1994 [12]. In this paper, based on PC1D-simulations, two kinds of departures are reported, which are 'departure 1' appearing for strongly injection level-dependent recombination, e.g. at an oxidized backside, and 'departure 2' appearing for significant recombination in the bulk and/or at the backside. We believe that for our cell departure 2 is active, since the bulk recombination is only weakly injection level-dependent ($n_1$ still very close to unity), but there is significant recombination at the Al back contact and in the multicrystalline bulk. According to [12] this deviation leads to an additional current-dependent recombination path and may be described by an additional contribution to the parallel conductance and/or to the second diode ($J_{02}$, $n_2$). Since this effect depends on the current density, it becomes negligible at low illumination intensity, which has been observed e.g. also in [10]. Hence, if this departure from the superposition principle holds (which should be the case for all industrial solar cells), it cannot be expected that the two-diode evaluation of illuminated characteristics leads to the same values of $J_{02}$, $n_2$ and/or $R_p$ as the evaluation of the dark characteristic. This departure from the superposition principle leads to a systematic reduction of the fill factor, which has nothing to do with the series resistance and cannot be explained only from the dark characteristic. Note that Fong et al. [11] have not observed this effect, which was probably due to the fact that they have investigated only monocrystalline high-efficiency type cells. Therefore, we propose here to fit the $R_s$ corrected and $J_{sc}$ shifted illuminated characteristic for full illumination intensity by a two-diode model, independent of the results of the fit of the dark characteristic. Fig. 6(a) shows the result of this fit (black dash-dotted line), and Table 2 contains the two-diode parameters obtained for the two illumination intensities. Since we already have adjusted $n_1$ to lead to the correct value of $V_{oc}$, this fit leads to the same value of $J_{01}$ as the dark fit did. This, together with the very good match between the measured and simulated curves in Fig. 6(a), indicates that our approach to describe the dark and the illuminated characteristic by the same two $R_s$ parameters is indeed correct.

As already mentioned before, the different parameters obtained from the $I$–$V$ curves characterizes effects with different physical origins [21]. The parameter $J_{01}$ mainly characterize the carrier lifetime in the bulk. There is an ongoing discussion whether the grain boundaries or intra-grain defects (dislocations) are most detrimental for solar cells. The presently dominating opinion is that the effect of the intra-grain defects is dominating, because the grain boundaries occupy only a negligible area fraction. However, it has been shown in [22] that in defect-rich regions of multicrystalline cells $J_{01}$ may be dominated by the grain boundaries. In contrast to this strong material-induced influence on $J_{01}$, the recombination current density, which is described by $J_{02}$ and $n_2$ in the dark $I$–$V$ curve, is essentially process-related, since it is mostly caused by extended defects crossing the p–n junction as cracks or badly passivated cell edges [21]. The $J_{02}$ and $n_2$-values obtained from the illuminated $I$–$V$ curve contain an additional recombination contribution due to the increased carrier density under illumination, as it was discussed before.

As it was done for the dark $I$–$V$ characteristic, additionally a conventional analysis based on the two-diode model with a fixed $R_s$ was made for the illuminated characteristic. In addition to fitting the measured illuminated characteristics data, the parameters of the dark characteristic were used to construct an illuminated characteristic, which was also analyzed, see lower part of Table 2. Again, here the ideality factor of the diffusion current is fixed to $n_1=1$ and thus the calculated $V_{oc}$ is 610.7 mV being slightly below the measured value. The corresponding lumped dark $R_s$ is 0.85 Ω cm$^2$ (see Table 2) and is still in the same range as the current-dependent $R_s^{dark}$ (see Fig. 5). Since the $R_s^{ill}$ is in reality even higher, also the fill factor $FF$ and the efficiency

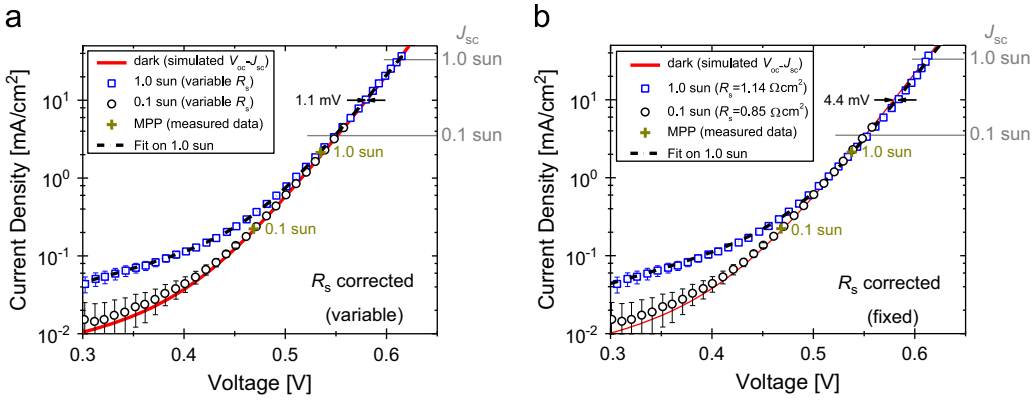


**Fig. 6.** Measured illuminated $I$–$V$ characteristics at 1.0 sun and 0.1 sun with a) current-dependent $R_s$ correction and b) fixed $R_s$ correction in comparison with the simulated $R_s$ corrected dark $I$–$V$ characteristic ($V_{oc}$–$J_{sc}$).

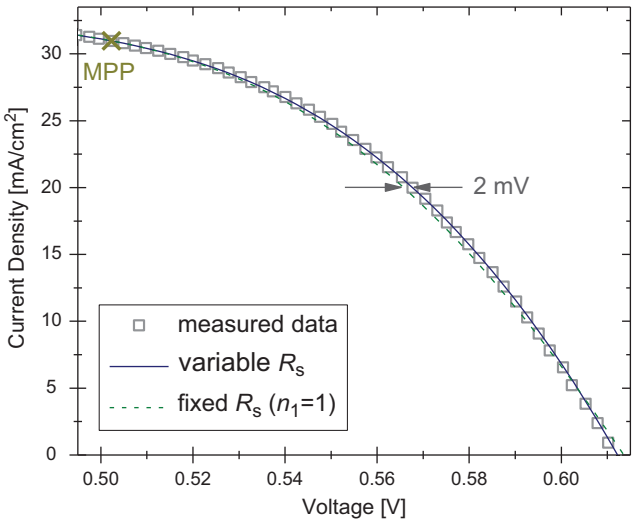


**Fig. 7.** Measured illuminated *I–V* characteristics at 1 sun fitted with current-dependent $R_s$ (solid, blue) and fixed $R_s$ (dashed, green). (For interpretation of the references to color in this figure legend, the reader is referred to the web version of this article.)

$\eta$ are overestimated in comparison to the measured values by this approach. To classify the data given in Table 2 it has to be noted that due to inaccuracies in the *I–V* curve measurement of about $\Delta V$=0.5 mV and $\Delta J$=0.01 mA/cm$^2$ the *FF* can just be evaluated up to a precision of about 0.2 %abs., which corresponds to an accuracy of about roughly 0.02 %abs. in $\eta$.

Fitting the illuminated *I–V* characteristic directly with fixed $R_s$, all parameters differ from that of the dark fit as given in Table 2. According to Fig. 6(b), the $R_s$ correction with resulting constant $R_s^{ill}$ does not lead to a straight line in the semi-logarithmic plot, thus the diode-equation cannot be fitted well and even $V_{oc}$ does not match the measured value. Even though the measured data around MPP are described well, the $R_s$ corrected measured data in Fig. 6(b) deviate by more than 4 mV from the characteristic simulated with fixed $R_s$ in the bias range between 550 mV and 600 mV. Therefore the influence of $R_s$ is overestimated by this approach. In comparison to the above introduced new method implying a variable $R_s$, the fit with fixed $R_s$ and $n_1$=1 on the illuminated *I–V* characteristic, especially in the voltage range above $V_{mpp}$, is clearly worse (see Fig. 7) and is not based on a meaningful parameter set describing dark and illuminated *I–V* curve at the same time. By evaluating the solar cell with an ideality factor $n_1$=1.03 (not shown here), the $J_{01}$ values of the dark and illuminated fit with fixed $R_s$ are almost the same ($J_{01}=2.82\times10^{-12}$ A/cm$^2$) and the $V_{oc}$ converges toward the measured once, but the fit in the bias range between 550 mV and 590 mV is still as poor as with $n_1$=1. Therefore it is obviously not possible to characterize the dark and illuminated *I–V* characteristic by the same set of two-diode parameters just with different but constant series resistance values for the dark and illuminated measurement. Applying the current-dependent $R_s$ approach extracts a meaningful parameter set and allows to estimate the illuminated *I–V* characteristic correctly based on measurements done in the dark. The departure from the superposition principle caused by the injection level-dependent recombination leads here to an overestimation of the *FF* of just 0.4 %abs. and thus a prediction of the efficiency up to an error of 0.1 %abs. can be expected.

## 6. Discussion

It has been shown by many authors and also by our comparisons that it is possible to fit dark and illuminated *I–V* characteristics of crystalline silicon solar cells separately, with an accuracy sufficient for most purposes, to a two-diode model implying a fixed series resistance. Then, however, at least if high currents are employed, the two-diode parameters become different between the dark and illuminated cases. We have shown here that this discrepancy is due to two different reasons. First, the distributed character of the series resistance influences the high-current part of both characteristics, thus leading to different values of $R_s$ and $J_{01}$. This may be regarded in good approximation by defining the global distributed series resistance of the cell $R_{dis}$ as a new parameter, in addition to the homogeneous series resistance $R_{hom}$. At low currents (below 0.1 $I_{sc}$) $R_{dis}$ is constant and has to be added to $R_{hom}$. For currents above 0.1 $I_{sc}$, $R_{dis}$ becomes current-dependent and may be described by the empirical formulas given in this paper, which also consider $R_{hom}$. The second reason for the deviations between dark and illuminated characteristics is the departure from the superposition principle described by Robinson et al. [12]. This departure is due to an additional current-dependent bulk recombination under illumination and is basically due to the fact that, at one and the same local bias, the minority carrier concentration in the bulk is higher under illumination and current extraction than in the dark. It should be mentioned that this departure is the physical reason why in photoluminescence (PL) imaging techniques always the PL image under short circuit condition has to be subtracted from all other PL images [5,23]. The minority carriers existing at zero local bias (short circuit) in the bulk just generate the recombination, which is responsible for the short circuit PL signal and for the additional current loss under illumination. Also this effect is dependent on the illumination intensity and becomes negligible for low intensities. This departure leads to significantly increased values of $J_{02}$ and $n_2$ and, in extreme cases, also to a reduced value for $R_p$ for the illuminated characteristic [12]. Hence, at least if the illuminated characteristic is measured under full illumination intensity, it cannot be expected that the second diode and $R_p$ parameters match that of the dark characteristic. These deviations are not due to the distributed character of $R_s$, these two mechanisms have to be clearly distinguished from each other. However, the values of $R_s$ and $J_{01}$ should be the same in the dark and under illumination for the consistent description of a solar cell, which is the case for our current-dependent $R_s$ approach introduced here.

The deviations appearing between the $R_s$ contributions obtained from EL $R_s$ and the fit of the current-dependent $R_s$ (see Fig. 1(c) and Table 1) are significant and need to be explained. It had already been mentioned that the EL data are based on the low-current approximation of the one-dimensional description of the distributed series resistance, which certainly does not hold for the 0.597 V/2.67 A measurement used for EL. According to this analysis, the value of $R_{hom}$ is significantly larger and that of $R_{dis}$ is significantly lower than that obtained from the analysis of the *I–V* characteristics. It has to be noted that the EL images underlying this analysis have been taken by using another sample stage than that used for measuring the *I–V* characteristics. It cannot be excluded that this stage did contribute slightly to the global series resistance, which could increase $R_{hom}$. Indeed, the current measured for the EL measurement (2.67 A) was significantly lower than that measured in the *I–V* characteristic, when $V_B$=597 mV was applied (3.04 A). Furthermore, the EL images analysis performed here did only consider the distributed resistance of the grid lines, but not that of the emitter. This may explain at least partly the higher $R_{dis}$ values obtained by evaluating the *I–V* characteristics. Finally, the whole EL analysis is based on the assumption of the validity of the so-called Fuyuki approximation [14,16,24]. This approximation says that the local EL signal is proportional to the local diffusion length $L_D$, and that the local $J_{01}$ is indirectly proportional to $L_D$. However, this proportionality was derived by Fuyuki et al. [24] only for solar cells being thick compared to $L_D$, which is not the case here. Moreover, this theory does not regard any depth-dependent

reabsorption of the EL radiation, which becomes important if the EL image is detected by a silicon detector, as in our case. One indication of the inaccuracy of the EL-based local $R_s$ values is given by the fact that the $R_s$ image shown in Fig. 1(a) obviously contains residues of the local lifetime distribution. Hence, a possible invalidity of the approximations underlying the EL-based $R_s$ analysis may lead to a serious deviation between the EL-based and the $I$–$V$ characteristics-based $R_s$ values. Finally, since the global $I$–$V$ characteristic has to be described by the ideality factor $n_1 = 1.06$, the same assumption was made in the EL $R_s$ procedure. However, we do not know whether this ideality factor is the same in all positions of the cell, which also might influence the EL evaluation.

It should be mentioned again that the two-diode model regarding a distributed series resistance introduced here is only applicable if the cell is essentially homogeneous. If it contains e.g. extended non-contacted regions showing a significantly increased local $R_s$, or if $J_{01}$ shows strong local inhomogeneities, it cannot be expected that our procedure will describe such a cell correctly. The method was applied for the evaluation of 5 cells, also with different grid design. Four of them show results similar to the presented example. The fifth cell shows a voltage difference between the dark and the reduced illuminated characteristic of about 6 mV. EL investigations of this cell according to [16] have revealed that it shows a strong local inhomogeneity in $J_{01}$ and therefore cannot be analyzed by the method mentioned above.

## 7. Summary and outlook

Within the two-diode model, a consistent description of the dark and illuminated characteristic is impossible with one and the same fixed series resistance, and it leads to residual discrepancies (e.g. different $J_{01}$ values) even if two different fixed series resistances are assumed. We have shown here that it is possible to describe the dark and illuminated $I$–$V$ characteristics very accurately by a single consistent set of diffusion current and $R_s$ parameters, if the distributed character of the series resistance is regarded. This procedure introduces only one additional parameter by splitting the series resistance $R_s$ into the two components $R_{hom}$ and the global distributed series resistance $R_{dis}$. The analysis proposed in this work consists of several steps. First, the dark characteristic up to a current value of about 0.1 $J_{sc}$ is conventionally fitted to a two-diode model assuming a constant $R_s$, leading to reliable values of $J_{01}$, $J_{02}$(dark), $n_2$(dark), and $R_p$(dark). For correctly matching the open circuit voltage, it is proposed to increase $n_1$ slightly until the suns-$V_{oc}$ characteristic calculated with these parameters matches $V_{oc}$ at $J_{sc}$. This measure is justified by the fact that, especially in multicrystalline solar cells, the lifetime is known to be dependent on the injection intensity [3,20]. Then, by comparing the suns-$V_{oc}$ with the measured dark characteristic for currents larger than 0.1 $J_{sc}$, the current-dependent dark series resistance is experimentally obtained and fitted to the empirical dependence (15), leading to the values of $R_{hom}$ and $R_{dis}$. Finally, by using these values and $J_{01}$ and $n_1$, the illuminated characteristic is fitted, leading to new values of $J_{02}$(ill.), $n_2$(ill.) and, in certain cases, probably also of $R_p$(ill.). The difference between these values and that obtained from the dark characteristic is due to the departure from the superposition principle described in [12].

The procedure proposed here will be implemented in a code for evaluating dark and illuminated $I$–$V$ characteristics, which will be made commercially available to the public [25].

## Acknowledgment

The authors are indebted to J. Greulich (Fraunhofer ISE, Freiburg, Germany) for providing the code used for the "conventional" fit of the dark and illuminated $I$–$V$ curves and to J.-M. Wagner (University Kiel) for valuable discussions. This work was financially supported by the German Federal Ministry for the Environment, Nature Conservation and Nuclear Safety and by industry partners within the research cluster "SolarWinS" (Contract no. 0325270C). The content is the responsibility of the authors.

## References

[1] O. Breitenstein, J. Bauer, K. Bothe, D. Hinken, J. Müller, W. Kwapil, M.C. Schubert, W. Warta, Can luminescence imaging replace lock-in thermography on solar cells? IEEE Journal of Photovoltaics 1 (2011) 159–167.
[2] C.T. Sah, R.N. Noice, W. Shockley, Carrier generation and recombination in p–n junctions and p–n junction characteristics, Proceedings of the IRE 45 (1957) 1228–1243.
[3] D. Macdonald, A. Cuevas, Reduced fill factors in multicrystalline silicon solar cells due to injection-level dependent bulk recombination lifetimes, Progress in Photovoltaics Research and Application 8 (2000) 363–375.
[4] S. Steingrube, O. Breitenstein, K. Ramspeck, S. Glunz, A. Schenk, P.P. Altermatt, Explanation of commonly observed shunt currents in c-Si solar cells by means of recombination statistics beyond the Shockley-Read-Hall approximation, Journal of Applied Physics 110 (2011) 014515.
[5] T. Trupke, E. Pink, R.A. Bardos, M.D. Abbott, Spatially resolved series resistance of silicon solar cells obtained from luminescence imaging, Applied Physics Letters 90 (2007) 093506.
[6] G.L. Araújo, A. Cuevas, J.M. Ruiz, The effect of distributed series resistance on the dark and illuminated current–voltage characteristics of solar cells, IEEE Transactions on Electron Devices 33 (1986) 391–401.
[7] B. Fischer, P. Fath, E. Bucher, Evaluation of solar cell $J(V)$-measurements with a distributed series resistance model, in: Proceedings of the 16th European Photovoltaic Solar Energy Conference, Glasgow, 2000, pp. 1365–1368.
[8] P.P. Altermatt, G. Heiser, A.G. Aberle, A. Wang, J. Zhao, S.J. Robinson, S. Bowden, M.A. Green, Spatially resolved analysis and minimization of resistive losses in high-efficiency Si solar cells, Progress in Photovoltaics Research and Application 4 (1996) 399–414.
[9] A.G. Aberle, S.R. Wenham, M.A. Green, A new method for accurate measurements of the lumped series resistance of solar cells, in: Proceedings of the 23rd IEEE Photovoltaic Specialists Conference, Louisville, 1993, pp. 133–139.
[10] J. Greulich, M. Glatthaar, S. Rein, Fill factor analysis of solar cell's current–voltage curves, Progress in Photovoltaics Research and Application 18 (2010) 511–515.
[11] K.C. Fong, K.R. McIntosh, A.W. Blakers, Accurate series resistance measurement of solar cells, Progress in Photovoltaics Research and Application (2011) 〈http://dx.doi.org/10.1002/pip.1216〉.
[12] S.R. Robinson, A.G. Aberle, M.A. Green, Departures from the principle of superposition in silicon solar cells, Journal of Applied Physics 76 (1994) 7920–7930.
[13] M. Glatthaar, J. Haunschild, M. Kasemann, J. Giesecke, W. Warta, Spatially resolved determination of dark saturation current and series resistance of solar cells, Physica Status Solidi (RRL) 4 (2010) 13–15.
[14] J. Haunschild, M. Glatthaar, M. Kasemann, S. Rein, E.R. Weber, Fast series resistance imaging for silicon solar cells using electroluminescence, Physica Status Solidi (RRL) 3 (2009) 227–229.
[15] K. Ramspeck, K. Bothe, D. Hinken, B. Fischer, J. Schmidt, R. Brendel, Recombination current and series resistance imaging of solar cells by combined luminescence and lock-in thermography, Applied Physics Letters 90 (2007) 153502.
[16] O. Breitenstein, A. Khanna, Y. Augarten, J. Bauer, J.-M. Wagner, K. Iwig, Quantitative evaluation of electroluminescence images of solar cells, Physica Status Solidi (RRL) 4 (2010) 7–9.
[17] S. Rißland, O. Breitenstein, Evaluation of luminescence images of solar cells for injection-level dependent lifetimes, Solar Energy Materials and Solar Cells, http://dx.doi.org/10.1016/j.solmat.2012.12.024, in press.
[18] 〈http://www.wolfram.com/mathematica/〉.
[19] A. Kassis, M. Saad, Analysis of multi-crystalline silicon solar cells at low illumination levels using a modified two-diode model, Solar Energy Materials and Solar Cells 94 (2010) 2108–2112.
[20] B. Michl, M. Rüdiger, J.A. Giesecke, M. Hermle, W. Warta, M.C. Schubert, Efficiency limiting bulk recombination in multicrystalline silicon solar cells, Solar Energy Materials and Solar Cells 98 (2012) 441–447.
[21] O. Breitenstein, J. Bauer, P.P. Altermatt, K. Ramspeck, Influence of defects on solar cell characteristics, Solid State Phenomena 156–158 (2010) 1–10.
[22] S. Rißland, O. Breitenstein, High resolution saturation current density imaging at grain boundaries by lock-in thermography, Solar Energy Materials and Solar Cells 104 (2012) 121–124.
[23] M. Glatthaar, J. Haunschild, R. Zeidler, M. Demant, J. Greulich, B. Michl, W. Warta, S. Rein, R. Preu, Evaluating luminescence based voltage images of silicon solar cells, Journal of Applied Physics 108 (2010) 014501.
[24] T. Fuyuki, H. Kondo, T. Yamazaki, Y. Takahashi, Y. Uraoka, Photographic surveying of minority carrier diffusion length in polycrystalline silicon solar cells by electroluminescence, Applied Physics Letters 86 (2005) 262108.
[25] 〈http://www.max-planck-innovation.de/en〉.